Effect of R substitution in Spin Glass $RFeTi_2O_7$ compounds

Arauzo A.[1,2], Bartolomé J.[2], Drokina T.V.[3], Petrakovskii G.A.[3], Molokeev M.S [3, 4]

[1]Servicio de Medidas Físicas, Universidad de Zaragoza, E-50009 Zaragoza, Spain
[2]Instituto de Ciencia de Materiales de Aragón (ICMA) and Departamento de Física de la Materia Condensada, CSIC- Universidad de Zaragoza, 50009 Zaragoza, Spain
[3]Kirensky Institute of Physics, Federal Research Center KSC SB RAS, Akademgorodok, 50/38, Krasnoyarsk, 660036, Russia
[4]Siberian Federal University, Krasnoyarsk, 660041, Russia

Abstract. Zirconolite oxides $R^{3+}Fe^{3+}Ti_2O_7$ (R rare earth element) are known to exhibit spin glass behaviour at low temperatures. Here we present a detailed study of these compounds for R = Eu, Gd, Dy, Ho, and Er, together with reviewed previous measurements on Sm, Tb, Tm, Yb and Lu, with the scope of determining the role played by the rare earth on their magnetic properties. They have been investigated using X-ray powder diffraction, and further characterized by magnetization, frequency dependent ac susceptibility and heat capacity measurements. $RFeTi_2O_7$ compounds are all isostructural showing orthorhombic structure, space group *Pcnb* at 300 K. Disorder of the magnetic ions in the $RFeTi_2O_7$ lattice induces spin glass behaviour at low temperatures, mainly due to the Fe sublattice. We show that magnetic rare earth ions participate in the spin glass state tuning its properties. In particular, the increase in the spin-glass temperature ΔT_{SG}^{R} with respect to the $LuFeTi_2O_7$, where Lu is non-magnetic, correlates with the de Gennes factor multiplied by the ratio of exchange interactions J_{RFe}/J_{FeFe}. Besides, for increasing anisotropy the spin glass transition dynamics slows down to values typical of cluster glass. The coercive field below the transition is increased in the same trend. Observed variations are explained as due to the anisotropic part of the R-Fe exchange interaction.

1 Introduction

The physics of spin glass systems has been a field of scientific interest in the last decades [1][2][3][4][5]. There is a large variety of materials showing spin glass behaviour or exhibiting spin-glass-like features, being the current experimental and theoretical research on this field of great interest. The study of new spin-glass materials and their behavior may reveal interesting physical properties.

In canonical spin glasses, a 3d transition metal magnetic impurity is dissolved in a nonmagnetic noble metal host. In these systems the interaction between localized moments is mediated by conduction electrons through the long-range isotropic so-called RKKY interaction. Most of the anisotropy in canonical spin-glasses comes from the much weaker Dzyloshinskii-Moriya interaction. On the contrary, insulating spin glasses contain high concentration of magnetic ions presenting short range interactions which can be isotropic or anisotropic [5]. Antiferromagnetic (AFM) superexchange interactions are dominant in the magnetic oxide spin glasses, with the exception of Eu^{2+} containing oxides, where FM interactions are predominant [6][7].

Examples of insulating spin glasses containing either 3d metals or 4f rare earth ions are abundant [5][3]. Numerous are the studies of spin-glass phase in transition-metal oxides, in manganites [8][9][10], cobaltites [11], and cuprates [12][13], among others. Spin glass behaviour is found in highly anisotropic 3d-metal heterometallic oxyborates like warwickites, which are naturally disordered materials [14]. Mixed crystals $Eu_xSr_{1-x}S$ with Eu^{2+} rare earth ion are well-known examples of Heisenberg spin glasses [15]. However the number of studies of spin glasses containing both 3d and 4f ions is scarce [6].

Within this framework, rare-earth zirconolite oxides with general chemical formula $R^{3+}Fe^{3+}Ti_2O_7$ (R-rare earth element) can serve as model materials for the study of disordered systems and spin glass magnetism. These compounds conjugate the possibility of cation substitution with the presence of crystal lattice disorder together with competing magnetic interactions [16][17][18][19][20].

The $LuFeTi_2O_7$ compound serves as reference example, where Lu is non-magnetic, to show characteristic spin glass behaviour. Dc magnetic susceptibility measured in zero-field cooled (ZFC) and field-cooled (FC) conditions deviate from each other

below the freezing temperature T_f = 4.5 K, ac susceptibility is frequency dependent, and heat capacity presents a rounded bump at that temperature range. Combining these results with X-ray diffraction and Mössbauer spectroscopy it was argued that the spin glass behavior stems from the disorder of the Fe atoms located at the different crystallographic positions [16][21].

The spin glass behaviour is maintained upon substitution of Lu by Sm [19], Gd [22], Tb [16], Dy [18], Tm [17], and Yb [20]. All of these compounds have similar magnetic spin glass behaviour, albeit dependent in detail on the lanthanide substitution.

The role of the presence of rare earth in spin glasses is important in binary metallic glasses [23], or in manganites [24][5]. The R=Pr and Nd doping induces structural modifications and magnetic anisotropy gives rise to anisotropic spin glasses [25], since their atomic radius varies along the series, affecting the interatomic distances and hence, their magnetic phases. Besides, spin glass behavior has also been found in other aluminoborates containing Fe and R, where a dependence on the freezing temperature was observed depending on the Fe/R ratio [6].

The purpose of this paper is to deepen on the understanding of the effect of the different magnetic rare earths on the spin glass behaviour of these series, depending on the R magnetic moment, and anisotropy.

For this purpose, besides the previously published results on the R = Sm [19], Gd [22], Tb [16], Dy [18], Tm [17], Yb [20], and Lu [18], mentioned above, we have carried out an analysis of the new compounds with R=Eu, Er and Ho, and complemented the study on R=Gd and Dy. Within this study we analyse the role of rare earth ions, providing a plethora of anisotropy types, in the behaviour of insulating spin glasses combining transition metal and rare earth elements. The magnetization as a function of field, dc and ac susceptibilities, and heat capacity measurements have been performed to account for the effect of R substitution in the $RFeTi_2O_7$ compounds.

2 Experimental Details

Powder samples of $RFeTi_2O_7$ (R = Eu, Gd, Dy, Ho and Er) were prepared by the solid state reaction method from a stoichiometric mixture of oxides Fe_2O_3, TiO_2, R_2O_3. The samples, formed in pellets, were subjected to a high-temperature treatment at 1250ºC. The chemical and phase compositions of the samples milled into powder were controlled by X-ray analysis.

The X-ray powder diffraction patterns of $RFeTi_2O_7$ samples for Rietveld analysis were collected on a Bruker D8-ADVANCE diffractometer (Cu-Kα radiation) with linear VANTEC detector at room temperature. All refinements of the patterns were performed with TOPAS 4.2 (Bruker).

Polycrystalline $RFeTi_2O_7$ magnetization measurements were carried out by a superconducting quantum-interference device (SQUID) magnetometer in the temperature range of 2 - 300 K and external magnetic field of 50 and 500 Oe. The magnetization as a function of temperature was measured both in zero-field-cooled (ZFC) and field-cooled (FC) regimes.

Ac susceptibility measurements were performed in a SQUID magnetometer, in the frequency range 0.01 < f < 1400 Hz, with an exciting field of 4 Oe.

Heat capacity as a function of temperature was measured on pellets using a Quantum Design PPMS (Physical Properties Measurement System) in the temperature range 1.9 -300 K. The sample was fixed to the sample holder with Apiezon grease.

3 Results and Discussion

3.1 Structure of $RFeTi_2O_7$

The structures of the synthesized $RFeTi_2O_7$ (R = Eu, Gd, Dy, Ho and Er) crystals have been determined from data of an X-ray diffraction experiment performed for a powder sample. The previously X-ray studied $GdGaTi_2O_7$ [15] was taken as the initial model for the determination of the crystal structure and atomic positions. The X-ray diffraction pattern of the crystal structure of $RFeTi_2O_7$ collected at room-temperature is shown in Fig. 1 for R = Eu, Gd, Ho and Er.

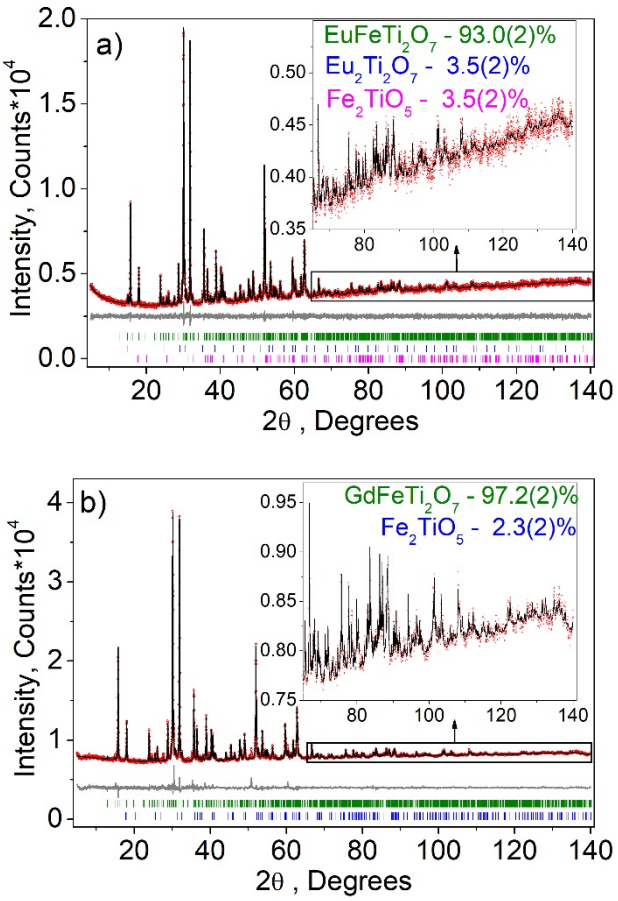

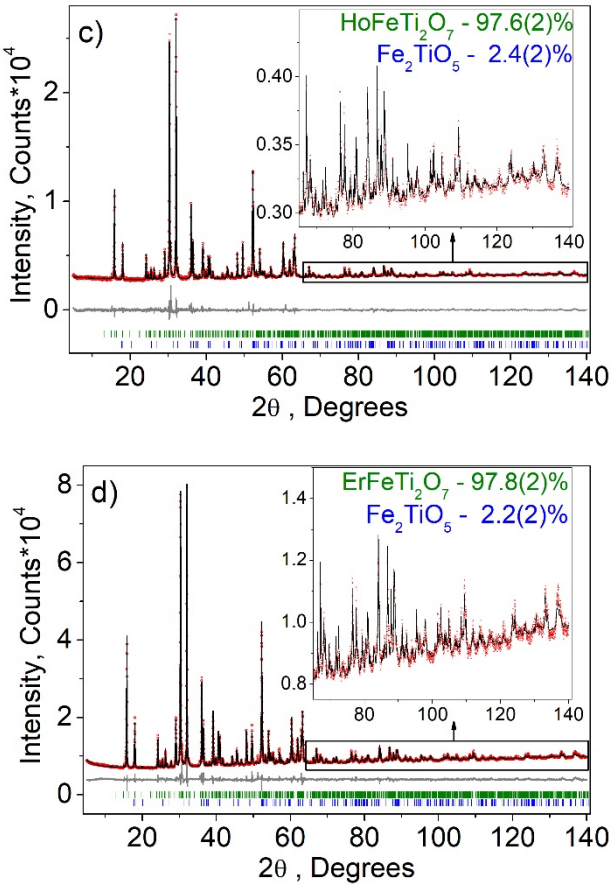

Fig. 1. *Experimental (symbols), theoretical (line), and difference (lower line) X-ray diffraction patterns of the crystal structure of $RFeTi_2O_7$ samples collected at room temperature. a) $EuFeTi_2O_7$, b) $GdFeTi_2O_7$, c) $HoFeTi_2O_7$ and d) $ErFeTi_2O_7$. The substance under study contains a small percentage of the Fe_2TiO_5 impurity (see inset).*

According to X-ray diffraction data the prepared compounds crystallize in the orthorhombic crystal structure, with space group *Pcnb*, at room temperature. A small amount of the impurity Fe_2TiO_5 (2-4%) was found in the substances. The key structural parameters of the compounds $RFeTi_2O_7$ (R = Eu, Gd, Dy, Ho and Er) and X-ray experimental details are given in Table I. Atomic coordinates and thermal parameters are presented in Table SI. The schematic crystal structure of $RFeTi_2O_7$ compound is shown in Fig. 2.

Occupation probability *p* of all ions after refinement is presented in Table SI. The unit cell of $RFeTi_2O_7$ is constructed by four-vertex, five-vertex, six-vertex, and eight-vertex oxygen polyhedra; the rare earth cation is arranged in the eight-vertex polyhedron. There are five nonequivalent iron sites: the two iron positions in the oxygen octahedron consisting of the Fe_t tetrahedron and Fe_f (Fe', Fe") five-vertex polyhedron, and the three positions ((Ti1/Fe1), (Ti2/Fe2), and (Ti3/Fe3)) in the mixed octahedral (see Fig. 2, a and b). The populations of the mixed Ti-Fe sites are different (Table SI). The tetrahedral sites are populated with Fe. These Fe atoms may be located out of the tetrahedra and populate neighboring sites Fe' and Fe" with coordination of five (Fig.2). Thus the peculiarities of the titanate structure indicate a disorder of the magnetic iron ions distribution mainly over five structural sites in $RFeTi_2O_7$ compound.

Table I. *$RFeTi_2O_7$. Crystallographic parameters at T = 300 K.*

Complex CCDC COD	$EuFeTi_2O_7$ 190039	$GdFeTi_2O_7$ 190038	$DyFeTi_2O_7$ 1529335	$HoFeTi_2O_7$ 190040	$ErFeTi_2O_7$ 1900752
Space group *Pcnb*					
a , Å	9.8356(2)	9.8321(2)	9.8467(2)	9.8353(2)	9.8285(1)
b, Å	13.6708(2)	13.6498(2)	13.5747(2)	13.5572(2)	13.5428(2)
c, Å	7.4491(1)	7.4250(1)	7.3650(1)	7.3497(1)	7.3378(1)
V, Å^3	1001.61(3)	996.49(3)	984.44(3)	980.01(3)	976.70(2)
Z	8	8	8	8	8
D_x, g/cm^3	5.533	5.639	5.811	5.796	5.860
μ, mm^{-1}	137.302	136.645	135.286	78.909	80.795
Radiation	Cu-*Kα*	Cu-*Kα*	Cu-*Kα*	Cu-*Kα*	Cu-*Kα*
2θ-range, deg.	5–140	5–140	5–140	5–140	5–140
Number of reflections	958	944	942	939	933
Number of refined parameters	82	84	73	82	73
R_{wp}, %	1.72	1.128	1.084	1.187	2.40
R_{exp}, %	1.58	0.577	0.573	0.915	1.04
R_p, %	1.36	0.995	1.112	1.657	1.59
GOF (χ)	1.09	1.956	1.892	2.063	2.31
R_{Bragg}, %	0.29	0.424	1.38	0.780	0.87

Note: V is the unit cell volume, Z is the number of formula units in the cell, D_x is the calculated density, μ is the absorption coefficient, Rwp is the weight profile uncertainly factor, R_{exp} is the expected uncertainly factor, R_p is the profile uncertainly factor, *GOF* (χ) is the adjustment quality, and R_{Bragg} is the Bragg integral discrepancy factor.

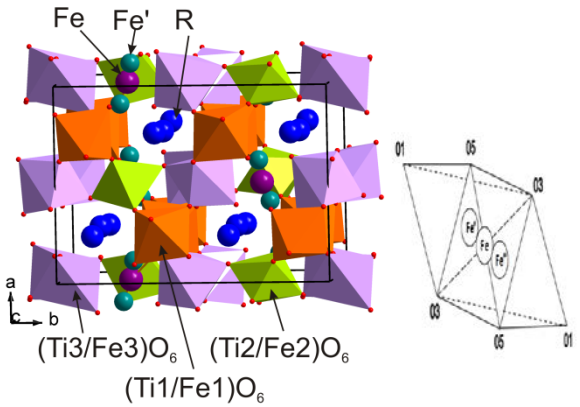

Fig. 2. *$RFeTi_2O_7$. The schematic crystal structure (left) and its fragment (right).*

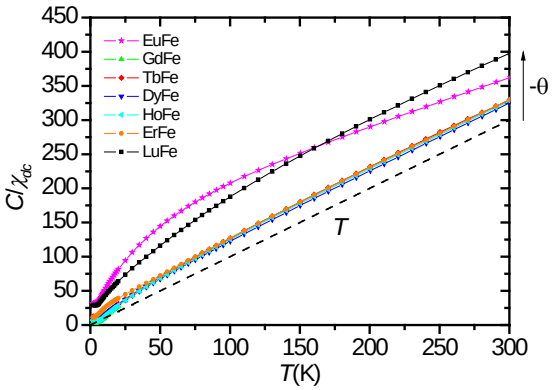

Fig. 3. *Temperature dependence of the inverse magnetic susceptibility of $RFeTi_2O_7$ (denoted 'RFe' in legend) multiplied by the obtained Curie-Weiss constant C for each rare-earth substitution (H = 0.5 kOe). The dashed line represents a Curie-Weiss temperature dependence fit defined by $C/\chi = T - \theta_N$ (for Neel asymptotic temperature $\theta_N = 0$ K).*

So, X-ray diffraction measurements show that the $RFeTi_2O$ compounds crystallize in the orthorhombic crystal structure, with space group *Pcnb*. The rare earth cation substitution does not change the crystal structure symmetry. The availability of the different non-equivalent positions for the magnetic Fe^{3+} ions in the unit cell induces structural disorder. Crystallographic data (excluding structure factors) for the structural analysis have been deposited with the Cambridge Crystallographic Data Centre, Nos CCDC-190038 ($GdFeTi_2O_7$), CCDC-190039 ($EuFeTi_2O_7$), CCDC- 1900752 ($ErFeTi_2O_7$) and CCDC-190040 ($HoFeTi_2O_7$). Crystallographic data for $DyFeTi_2O_7$ has been deposited in the Crystallography Open Database with No. COD-1529335.

3.2 Magnetic Properties

3.2.1 Dc Magnetic susceptibility

The temperature dependence of the magnetic susceptibility in an external magnetic field of 0.5 kOe has been measured for $RFeTi_2O_7$ (R = Eu, Gd, Dy, Ho and Er). The inverse magnetic susceptibility $1/\chi$ has been fitted to a Curie-Weiss law in the $150 \leq T \leq 300$ K range. Obtained parameters are included in Table II. All the studied compounds show negative Neel asymptotic behaviour, indicating that the dominant interaction is antiferromagnetic. In Fig.3 the $C/\chi = T-\theta$ temperature dependence is depicted for every compound, where C is the obtained Curie-Weiss constant obtained in the fit (see Table II). For the sake of comparison, data for R=Tb and Lu, measured and published in a previous study by our group [16], have been used in the analysis.

It is clearly observed that all the rare earth compounds, except for R=Eu, follow a T slope at high temperature. The reason for the discrepancy in the case of Eu is that we have not considered a temperature independent contribution to the susceptibility which is large in the case of Eu^{3+} ion, due to the low lying excited states [26]. The experimentally determined effective magnetic moment for all the materials is given in Table II. These values of the effective moment contain the contribution from the rare earth ion and the Fe^{3+} ion, which we can consider as additive in the high temperature range. The value of the effective moment $\mu_{Fe} = 5.16 \pm 0.06\ \mu_B$ for the Fe sublattice in the $LuFeTi_2O_7$ compound (Lu non-magnetic) may be used to determine the values of the experimental effective moment μ_R for the other R substitutions through the expression:

$$\mu_R = (\mu_{eff}^2 - \mu_{Fe}^2)^{1/2} \qquad [1]$$

Table II. *Obtained parameters for the fit of the $\chi^{-1}(T)$ experimental values to a Curie-Weiss law, C and θ. Calculated effective moment of the different compounds, μ_{eff}, and rare-earth effective moment, μ_R in μ_B units. *Values derived from experimental data from previous study* [16]. *Previously reported values for Sm, Tm and Yb have been also included.*

Ln	C (emuK/mol)	θ (K)	$\mu_{eff}(\mu_B)$	$\mu_R(\mu_B)$
Sm[19]	3.7	-95	5.55	2.04
Eu	4.7±0.4	-134±14	6.2±0.2	3.4±0.5
Gd	10.8±0.1	-30±3	9.28±0.04	7.71±0.09
Tb*	14.9±0.1	-31±2	10.93±0.05	9.63±0.10
Dy	17.0±0.1	-25±1	11.68±0.02	10.48±0.05

Ho	17.0±0.1	-28±1	11.68±0.04	10.47±0.09
Er	14.8±0.1	-30±2	10.87±0.04	9.56±0.08
Tm[17]	10.4	-43	9.11	7.51
Yb[20]	7.0	-127	7.48	5.41
Lu*	3.3±0.1	-100±8	5.16±0.06	0.00

The experimental values obtained agree excellently with the expected values for free *R*, according to Hund´s rule (see Fig. 4).

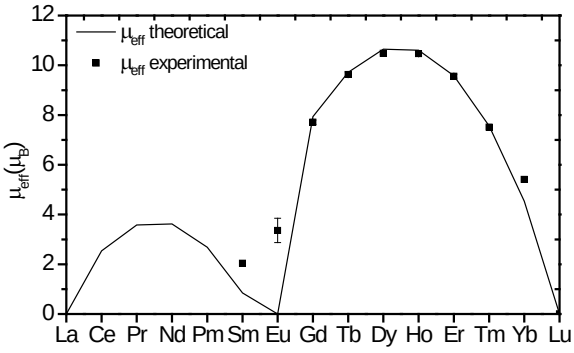

Fig. 4*. Experimentally determined effective moment for the different measured lanthanides in $RFeTi_2O_7$, μ_R compared to theoretical prediction $\mu_{eff} = g_J\sqrt{J(J+1)}$. Already published data for Sm* [19]*, Tm* [17]*, and Yb* [20]*, have been added to the graph.*

The above agreement is rather good for most of the rare earth ions. Let us remember that we are analyzing the macroscopic magnetic susceptibility of polycrystalline samples at high temperatures. In fact, the crystal field interaction which generally splits the ground state J multiplets, determining the collective temperature behavior mainly at low temperatures, is not considered at the present stage of analysis. In our naïve approach we estimate the overall average contribution at temperatures near room temperature considering that all the CF split levels are populated. The obtained estimation of the effective interaction given by Neel asymptotic temperature θ_N may differ from the interaction determined at low temperature, which is, in general, anisotropic.

As temperature decreases, the $\chi(T)$ behavior strongly deviates from a Curie-Weiss law, due to depopulation of crystal field split levels and magnetic interaction effects. There are no previous studies of R^{3+} single ion anisotropy in $RFeTi_2O_7$ compounds. According to the X-ray diffraction data, all compounds are isostructural to Zirconolite structure, $CaZrTi_2O_7$. It is built from four, five, six, and eight-vertex polyhedra. The eight-vertex polyhedron contains a rare earth ion [22]. The zirconolite structure can be considered as a derivative of the $A_2B_2O_7$ pyrochlore structure, where A and B represent large 8-coordinate and small 6-coordinate cations, respectively [27]. Although there are important differences in the coordination symmetry of the rare earth ion in both structures, we can consider the extensive and numerous studies of the rare earth crystal field in pyrochlores as a reference of the anisotropy of the ground state [28] [29][30][31][32][33][34][35][36]. Dy^{3+}, Tb^{3+}, and Ho^{3+} are very anisotropic in rare-earth titanates $R_2Ti_2O_7$ [29]. Dy^{3+} is a good realization of the spin-ice model with the ground-state wave function completely dominated by $|^6H_{15/2}, \pm 15/2>$ states (Kramers doublet). Ho^{3+} also shows Ising anisotropy at low temperatures, with a ground state doublet dominated by $|^5I_8, \pm 8>$ components. Tb^{3+} ground state has again an Ising character, with the ground state doublet mainly composed of the $|^7F_6, \pm 4>$ components. The lowest excited level in Tb^{3+} is at only 17 K, quite low in comparison with Dy^{3+} and Ho^{3+} where it lies at more than 200 K [29]. Therefore Ho and Dy present extreme axial anisotropy. Er and Yb show easy plane anisotropy for the ground state and are usually labeled XY-type. For Yb^{3+} the anisotropy persists up to high temperature because excited Kramers doublets lie at high energy (700-1000K) [31]·[32]. Tm ion has a singlet ground state and Gd is isotropic down to very low temperatures.

Magnetization measurements as a function of temperature both in zero-field-cooled (ZFC) and field-cooled (FC) regimes for external magnetic field H = 0.05 kOe show a bifurcation at low temperatures for all measured compounds, which is a revealing characteristic for spin glasses at the freezing temperature T_f (see Fig. 5). Similar behaviour in $M(T)$ at H = 0.5 kOe has been observed for Sm [19], Tm [17], and Yb [20]. ZFC/FC curves of $RFeTi_2O_7$ for magnetic R cannot be explained in terms of a superposition of the spin glass behavior of the Fe^{3+} sublattice and a paramagnetic behavior of the R^{3+}. The large deviation observed between ZFC and FC curves as compared to $LuFeTi_2O_7$ clearly indicates that rare earth magnetic sublattice is magnetically coupled to the iron sublattice. Even for the $ErFeTi_2O_7$ where no maximum is observed, the splitting of the curves is one order of magnitude larger than for Lu substitution. The so obtained freezing temperature, defined as the temperature below which irreversibility is observed, depends on the rare earth ion, varying from 2.6 K for $GdFeTi_2O_7$ to 6.5 K for $TbFeTi_2O_7$. Additionally, the degree of irreversibility (relative divergence between ZFC and FC curves), is strongly *R*-dependent, being larger for the *R*=Tb, Dy and Ho substitutions as compared with that in the Lu, Gd, Eu and Er (see Fig. 5). The reason for this behavior stems from the larger anisotropy induced by the presence of the *R* in the former cases, since it is known that with an 8 fold coordination of O atoms, for example in $R_2Ti_2O_7$ pyrochlores [29], the anisotropy of the Tb, Dy and Ho is strongly uniaxial, while that of Er and Yb tend to XY, and Eu and Gd are isotropic. We confirm this statement below.

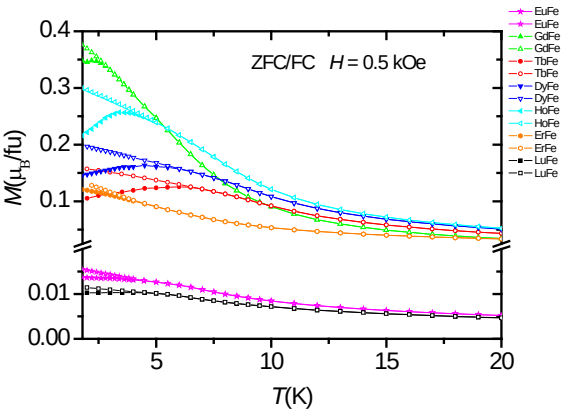

Fig. 5*. Temperature dependence of the magnetization M(T) (ZFC (solid symbols) and FC (open symbols) curves at an external magnetic field H = 0.5 kOe in $RFeTi_2O_7$ (R=Eu, Gd, Dy, Ho and Er) together with $TbFeTi_2O_7$ and $LuFeTi_2O_7$ results* [16].

Additionally, it has been found in $GdFeTi_2O_7$ that the freezing temperature T_f of this spin system depends strongly on the value of the external magnetic field H: T_f = 2.6 K at H = 0.5 kOe and T_f = 4.5 K at H = 0.05 kOe (Fig. 6). This means that the spin-glass freezing has a peculiar sensitivity to an external magnetic field in $GdFeTi_2O_7$ system. We have observed such a field dependence of the T_f in the other R compounds, although to a lower extent.

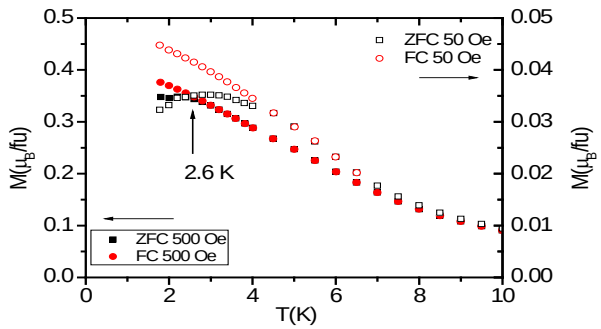

Fig. 6. *$GdFeTi_2O_7$. Temperature dependence of the magnetization M(T) (ZFC (open squares) and FC (open circles) curves at an external magnetic field H = 0.05 kOe and ZFC (solid squares) and FC (solid circles) at an external magnetic field H = 0.5 kOe).*

The magnetic phase diagram in the temperature and magnetic field plane has special interest in the study of magnetic anisotropy effects of spin glasses. They are classified according to the type of their magnetic interactions in Ising, XY or Heisenberg models. For Ising-like spin glasses, it is theoretically predicted that an equilibrium spin glass transition persist in the presence of a magnetic field, and the in-field transition line called the Almeida and Thouless (AT) line behaves as $H_c \alpha (T_c - T)^{3/2}$ (or $\delta T_f \propto H^{2/3}$) [37]. By contrast, in the fully isotropic Heisenberg case the in-field transition is associated with the transverse spin glass order set in at the so-called Gabay and Toulouse (GT) line behaving as $H_c \alpha (T_c - T)^{1/2}$ ($\delta T_f \propto H^2$) [38]. Unluckily, the observed variations of T_f with applied magnetic field could not be classified in terms of the above mentioned theoretical models given the complexity inherent to these compounds.

3.2.2 Magnetic field dependence of the Low Temperature Magnetization

The magnetization hysteresis curves $M(H)$ at T=2.0 K have been measured at -50 kOe<H<50 kOe. The $LuFeTi_2O_7$ has an antiferromagnetic behavior evidenced by the slope at the highest field, and a coercive field of H_c = 143 Oe. The presence of the magnetic R sublattice gives rise to an increase in the $M(H)$ value and an increase in the coercive field with the trend Er<Ho<Dy<Tb (see Fig. 7 inset). Although the highest value of $M(H)$ is achieved by the $GdFeTi_2O_7$, it has the lowest H_c of the series, even lower than the Lu compound. The exceptional behavior of the Gd substitution can be related to the very small Fe-Gd exchange interaction and its isotropic character, leading as a consequence to the magnetic softening of the $GdFeTi_2O_7$ compound. Thus, the above conjecture on the effect of the R anisotropy on the spin glass behavior is confirmed.

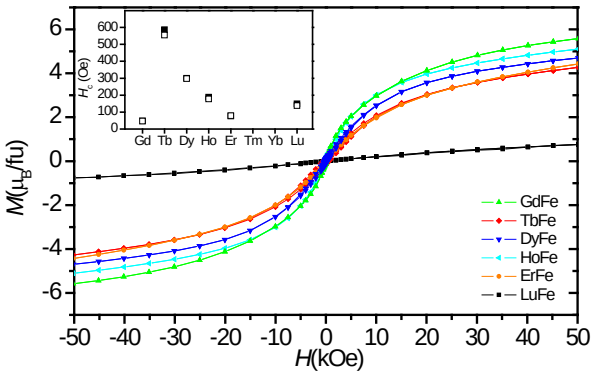

Fig. 7*.Hysteresis loop at 2.0 K up to 50 kOe for R=Gd, Tb. Dy, Ho, Er and Lu. Inset: Coercive field values, H_c (bold squares), -H_c (open squares).*

3.2.3 Ac susceptibility measurements

We have carried out a study of the dynamical properties of the spin glass transition by means of ac susceptibility. Moreover, this technique allows us determining the freezing temperature at very low magnetic field, given the spin-glass state sensitivity to magnetic field. The results of ac susceptibility measurements at different excitation frequencies f and fixed driving field amplitude of 4 Oe on the powder sample $ErFeTi_2O_7$ are shown in Fig. 8a, 8b. Very similar results are obtained for the other substitutions (see SI2). The onset of the spin glass transition is defined by a cusp in the in-phase susceptibility $\chi'(T)$ or by an inflection point in the out-of-phase component, $\chi''(T)$. We observe that in the whole series, except for the $LuFeTi_2O_7$ compound, the cusp in the $\chi'(T)$ is smeared out as frequency increases (see Fig. 8), therefore we have taken the well resolved maximum

slope in $\chi''(T)$ as the $T_f(f)$ onset. The freezing temperature varies with frequency, for instance, for $HoFeTi_2O_7$, freezing temperature increases from the lowest value $T_f \sim 6.7$ K at 0.1 Hz, to $T_f \sim 7.6$ K at the highest frequency measured, 1400 Hz (see Fig. 8). The experimental results for other R can be found in section S2 of Electronic Supplementary Information (ESI).

A way to evaluate the frequency sensitivity of freezing temperature is to calculate the p_f factor, defined as the relative shift in freezing temperature per decade of frequency, $p_f = \Delta T_f/[T_f \Delta(\log f)]$. Obtained values are given in Table III. It is observed that values for R = Lu, and Gd are rather low and within the range of values obtained in canonical spin-glasses: 0.005-0.018 [2]. However for Dy, Ho and Tb, the variation of T_f with frequency is larger, with p_f values of about 0.03 (see ESI, S3). Observed differences deserve a deeper analysis.

The values of $T_f(\omega)$ for the different R substitutions are depicted in Fig. 8c, and have been analysed within the Dynamical scaling theory near a phase transition at T_c. According to this theory, the relaxation time follows the critical slowing down law, which in terms of frequency predicts

$$f = f_0 (T_f(\omega)/T_c - 1)^{z\nu} , \qquad [2]$$

where $T_f(\omega)$ is the frequency dependent freezing temperature determined by the inflexion point in $\chi''(T)$ and T_c is the phase transition temperature in the limit of zero frequency, f_0 is the characteristic frequency constant, ν is the critical exponent for the correlation length ξ and z is the dynamical exponent. The obtained fit parameters are collected in Table III, together with those for the Lu and Tb substitutions. We note that the critical behavior of the different R provides a whole panoply of results. Isotropic Gd shows very similar results to Lu, with high values for f_0, indicating a fast relaxation process, typical of canonical spin-glasses [2]. On the other hand, Ising ions like Dy, Ho and Tb have a much lower f_0 parameter, which is characteristic of slower relaxation similar to values observed in cluster spin glasses [2][39][40][41][42]. Obtained values for T_c are very close, slightly lower, than the experimental value of T_f at the lowest frequency, taken as T_{SG} (column 3 in Table III), in excelent agreement to what it would be expected for the zero frequency transition temperature.

The slower relaxation obtained for the strongly anisotropic ions, Tb, Dy and Ho, means that the time constant for a spin flip is slowed down by the anisotropic interaction. This behaviour which is typical of clustering in spin glasses would indicate a stronger interaction between the rare earth and the iron for the more anisotropic ions.

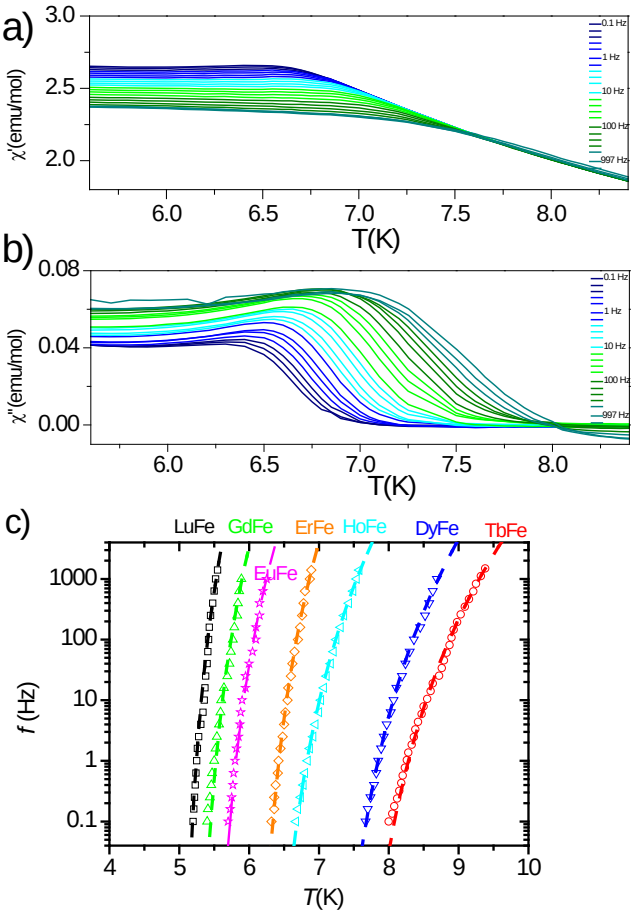

Fig. 8. *a) $HoFeTi_2O_7$. Temperature dependences of the in-phase component χ' and b) the out-of-phase component χ'' of ac magnetic susceptibilities using an ac magnetic field of 4 Oe as a function of frequency. c) Variation of the spin-glass transition temperature as a function of frequency for $RFeTi_2O_7$ (R=Eu, Gd, Dy, Ho and Er) compared to $TbFeTi_2O_7$ and $LuFeTi_2O_7$ results* [16]. *Dashed lines show the fit to a critical slowing down law.*

Table III. *Spin-glass transition temperature determined by dc at H = 0.5 kOe and ac susceptibility experiments (0.1 Hz, 4 Oe). Best fit parameters for the frequency dependence of the spin-glass transition.*

	T_f(K) 500 Oe	T_{SG}(K) ac	P_f	T_c(K)	f_o (Hz)	$z\nu$
EuFe	4.5±0.2	5.7±0.1	0.022	5.4±0.5	$3\pm1\cdot10^{10}$	9±1
GdFe	2.6±0.2	5.4±0.1	0.017	5.2±0.5	$7.0\pm0.3\cdot10^{10}$	9±1
TbFe	6.5±0.5	8.0±0.1	0.034	7.4±0.5	$2.1\pm0.1\ 10^{8}$	9±1
DyFe	6.0±0.5	7.7±0.1	0.029	7.1±0.5	$6.4\pm0.2\cdot10^{8}$	9±1
HoFe	5.0±0.5	6.7±0.1	0.029	6.2±0.1	$1.0\pm0.5\cdot10^{9}$	9±1
ErFe	5.0±0.5	6.3±0.1	0.020	6.0±0.5	$7\pm4\cdot10^{10}$	9±1
LuFe	4.5±0.2	5.2±0.1	0.014	5.0±0.5	$6\pm4\cdot10^{11}$	9±1

In the following analysis and discussion, we will take as spin-glass transition temperatures, T_{SG}, those obtained by ac magnetic susceptibility at the lowest frequency, 0.1 Hz (Table III, column 3), thus minimizing variations with applied magnetic field and frequency.

From the dynamical analysis of the freezing temperature we observe a clear dependence of the transition temperature and their dynamics with the anisotropy of the R ion. The same trend observed in H_c is repeated for the spin glass temperature, increasing in the series Er<Ho<Dy<Tb. The obtained characteristic spin flip relaxation time, $\tau_0 = 2\pi/f_0$, as well, is following the same trend, demonstrating how the rare-earth ion anisotropy is influencing the spin glass state in these materials.

3.3 Calorimetric Properties

Heat capacity measurements as a function of temperature were performed on the $LnFeTi_2O_7$ series. Data are presented in Fig.9. They show no peak associated with a magnetic ordering transition, instead there appears a very broad contribution with a maximum at about 5-10 K which can be ascribed to the spin-glass state. At low temperatures a linear dependence with temperature is observed, typical of spin glasses, related to the intrinsic spin disorder. The data shown in Fig. 9 have been extrapolated to very low temperatures (T < 2K) following the experimentally obtained T slope. The application of an external magnetic field smears out the contribution

For $GdFeTi_2O_7$ the associated magnetic entropy has been found to increase up to a maximum value of about 2.13 R at 50K (see Inset right Fig.9). This value is much lower than the molar entropy expected for a S = 5/2 Fe^{3+} ion and a S = 7/2 Gd^{3+} ion per formula unit, which is an indication of the multiplicity of the ground state typical of spin-glasses. It is remarkable the large increase of entropy in the Gd case, evidently ascribable to the larger Gd spin and its isotropic character.

A similar analysis can be made for the rest of compounds: in all cases the calculated entropy yields much smaller values than those expected for a regular magnetic ordering transition.

Taking the $LuFeTi_2O_7$ contribution as referent, the broad HC maximum is shifted towards lower temperatures for the Er substitution and to higher temperatures for Dy, Ho and Tb compounds, as would be expected for the larger T_{SG} values. Typically, magnetic specific heat in spin glasses shows a broad maximum centered at 20-40 percent above the transition [3], which agrees with observed contribution for the different complexes.

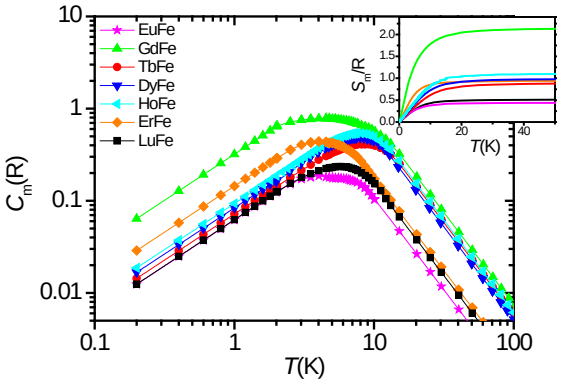

Fig. 9. *Temperature dependence of the magnetic contribution to the heat capacity, C_m, of $RFeTi_2O_7$, (R = Eu, Gd, Tb, Dy, Ho, Er and Lu). Values below 2K have been obtained by data extrapolation considering a linear T dependence. Inset: Calculated associated magnetic entropy, S_m.*

4. Discussion

The Weiss constants θ_W obtained from magnetic susceptibility measurements are collected in Table III. For the $LuFeTi_2O_7$ the Weiss constant for the Fe sublattice is obtained and denoted as θ_{Fe}. Since they are determined from a high temperature range where the high temperature correlations play a role, they may be used to evaluate the average Fe-Fe and Fe-R interactions. A mean field method for two different magnetic sublattices has been proposed earlier for RFe boroaluminates spin glasses that may be applied in the present case [6]. The two sublattice magnetic system in an applied field H can be modelled by the Hamiltonian:

$$\mathcal{H} = -\sum_{i>j}^{Fe} 2J_{Fe^i,Fe^j} S_{Fe^i} \cdot S_{Fe^j} - \sum_{i,j}^{Fe,R} 2J_{Fe^i,R^j} S_{Fe^i} \cdot S_{R^j}$$

$$-\sum_{i>j}^{R} 2J_{R^i,R^j} S_{R^i} \cdot S_{R^j} + g\mu_B H \sum_i S_{i,z} \qquad [3]$$

Where R is an RE ion, S_i is the spin operator at the i site, J_{ij} is the exchange constant of the magnetic interaction between the i and j sites, and g's are the Lande's factor. Assuming that at high temperature each R and Fe sublattices follow a Curie Weiss law in absence of the Fe and R sublattices, respectively:

$\chi_A(T) = \frac{C_A}{T-\theta_A}$, where C_A and θ_A are the Curie and Weiss constant, respectively, for ion A, and $\chi_{RFe}(T) = \frac{C_{Fe}+C_R}{T-\theta_W}$ for the two sublattice system. The following relation between the Weiss constants of the two sublattices is obtained

$$\theta_W = \frac{C_{Fe}\theta_{Fe}+C_R\theta_R+2(C_{Fe}C_R)^{1/2}\theta_{RFe}}{C_{Fe}+C_R} \qquad [4]$$

Assuming that the R^iR^j 4f-4f interaction is much weaker than between RFe, 4f-3d and Fe^iFe^j 3d-3d interactions, as

can be expected from the internal orbital of the R 4f electrons, the parameter θ_{RFe} can be extracted from the experimental data in Table II:

$$\theta_{RFe} = \frac{(\mu_{Fe}^2+\mu_R^2)\theta_W-\mu_{Fe}^2\theta_{Fe}}{2\mu_{Fe}\mu_R} \quad [5]$$

The results are given in Table IV. The average exchange interactions may be estimated within a next nearest neighbor scheme if the number of neighbors B to each atom A, $Z_{A,B}$, is known, as is the present case, if one takes account of the five types of sites, where Fe can be placed and their respective statistical weights (see S5, ESI). One obtains for $Z_{Fe,Fe}$ = 2.9, the value

$$\frac{J_{FeFe}}{k_B} = \frac{3\theta_{Fe}}{\mu_{Fe}^2\left(2Z_{Fe,Fe}/g^2\right)} = -7.8 \text{ K} \quad [6]$$

A similar expression is obtained for the average J_{RFe} interaction constant

$$\frac{J_{RFe}}{k_B} = \frac{3\theta_{RFe}}{\mu_R\mu_{Fe}\left(Z_{R,Fe}/g_R^2+Z_{Fe,R}/g^2\right)} \quad [7]$$

In this case, we distinguish between the average number of Fe atoms around R ion, $Z_{R,Fe}$=2.5 from R atoms around Fe Z_{FeR}=3.5 (see S5, ESI) . The exchange constants J_{RFe} are collected in Table IV. The positive value for Gd implies that this interaction is ferromagnetic (FM), while all the rest are antiferromagnetic (AFM), and are more than one order of magnitude weaker than the J_{FeFe} interaction. Thus, it can be expected that the Fe sublattice and its internal FeFe interaction are dominant in establishing the magnetic behavior of these systems, albeit, modulated by the presence of the R moments weakly coupled to the former.

Table IV. *Weiss interaction parameter θ_{RFe} calculated for the different lanthanides studied in this work. Values for Sm, Tm and Yb have been obtained from references* [19], [17], *and* [20] *respectively. Mean exchange constants of the magnetic interaction between R and Fe are given in units of k_B.*

Ln	θ_{RFe}(K)	J_{RFe}/k_B(K)
Sm	-12.5	-0.11
Gd	0.6±2.8	0.03±0.14
Tb	-10.4±3.0	-0.32±0.09
Dy	-7.3±1.4	-0.18±0.03
Ho	-11.0±1.5	-0.25±0.03
Er	-9.4±2.5	-0.22±0.06
Tm	-11.7	-0.33
Yb	-79.5	-3.06

For $LuFeTi_2O_7$ $T_{SG}^{Fe} = 5.2(5)K$, which serves as *R* non-magnetic reference for the other compounds. All of them T_{SG}^{R} are higher than T_{SG}^{Fe} . The difference $\Delta T_{SG}^{R} = T_{SG}^{R} - T_{SG}^{Fe}$ is depicted in Fig. 10.

To our knowledge, there is no developed theory available relating T_{SG} with the next neighbors interactions in a two sublattice model to explain this interesting dependence. However, in the case of magnetic correlations leading to a long range ordering at T_c the transition temperature of the RFe compounds $\Delta T_c^R = T_c - T_c^{Fe}$ also depend on the R substitution [43]. In that case it is shown that

$$\Delta T_c^R \sim {}^{GJ_{RFe}}/_{J_{FeFe}} \quad [8]$$

Where $G=(g_J-1)^2J(J+1)$ is de Gennes factor. We conjecture that since the correlations leading to the spin glass transition are caused by the exchange interactions, the T_{SG} dependence on *R* following this product may be expected. In Figure 10, we compare the product Eq. 8, of the Gennes factor with the ratio of the normalized interaction values, obtained in previous analysis (Table IV), with the experimentally obtained ΔT_{SG}^R. We observe good correlation with the experimental ΔT_{SG}^R.

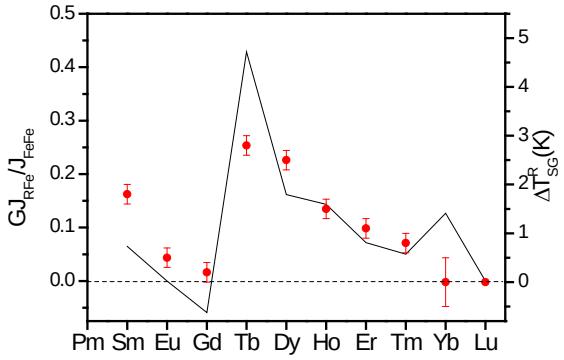

Fig.10. *Comparison of the R-dependence of the product $G(J_{RFe}/J_{FeFe})$ (black line, left axis) with the variation of the spin glass transition temperature, ΔT_{SG}^R (red circles, right axis).*

Therefore, we are able to explain the increase of the spin-glass temperature in $LuFeTi_2O_7$ when non-magnetic Lu^{3+} ion is replaced by another rare-earth, as due to increased magnetic correlations. An estimation of the average magnetic interactions between the rare earth ion and the iron sublattice at low temperature is done by calculating high temperature magnetic correlations within a mean field theory.

Let us dwell on the qualitatively different result (Ferromagnetic and small) obtained for the interaction in the case of isotropic Gd^{3+} with respect to the anisotropic substitutions. The d-f interaction has been proposed to consist of two components: an isotropic Heisenberg, and a non-Heisenberg anisotropic component, with both components competing when they are of opposite signs. [44]. We propose that in the $RFeTi_2O_7$ compounds the isotropic component is mainly determined from the Gd compound, while in the R=Er, Dy, Ho and Tb substitutions, the R-Fe exchange is dominated by the anisotropic component of the f-d exchange coupling.

This conjecture is based on the important role of non-Heisenberg exchange that has been demonstrated in orthoferrites, where the isotropic part of the exchange interaction is almost completely compensated by the AF ordering of the d ions (Fe^{3+}) [44]. Spectroscopic measurements showing the increase in the rare-earth ground state exchange splitting for the magnetic configuration stable at low temperatures indicate a larger anisotropic contribution for the more anisotropic R^{3+} ions.

Indeed, in the compounds under study, we find a dominant AF interaction in the Fe^{3+} sublattice, J_{FeFe}/k_B = -7.6 K, and therefore the calculated mean values for the J_{RFe}/k_B (see Table IV) can be considered an estimation of the anisotropic f-d exchange contribution.

The positive value found for the J_{RFe} in the case of Gd^{3+} might be a differentiating factor for this rare earth. Albeit the value is very low and within error bar, predominant FM interactions are also found for the isoelectronic ion Eu^{2+} in Eu^{2+} based oxide crystals, which are attributed to its electronic state [7].

On the other hand, it is also remarkable the discrepant value obtained for θ_{RFe} for R=Yb. This value is calculated with Eq. 3, taking as θ_W = -127 K experimentally determined from the χ^{-1} (T) fit in reference [20]. Such a high value for the asymptotic Neel temperature may be originated in the large crystal field splitting usually observed for Yb^{3+} as compared with the rest of studied magnetic R^{3+}. See for instance energy levels obtained in pyrochlore compounds [31][32]. Yb^{3+} ground state is a doublet with the first excited state lying at an energy of more than 700 K above Ground State. Up to room temperature, Yb^{3+} moment is regarded as an isotropic pseudospin S=1/2 [30]. Fit of the experimental $\chi(T)$ using the Crystal Field levels obtained by Inelastic Neutron Scattering in $Ba_3Yb_2Zn_5O_{11}$ yields an AF molecular field constant, λ = -9 mol/emu. That result is equivalent to an approximate value of $\theta_W = \lambda C$ =-23 K, in the Curie-Weiss formulation, whereas the high temperature asymptotic determination would yield a much larger value for θ_W [30]. This would explain the discrepancy observed in the calculated J_{RFe}/k_B for Yb (see Table IV).

In previous studies in these $RFeTi_2O_7$ compounds it had been argued that the spin glass state was associated to frustration caused by the competitive magnetic interactions between Fe^{3+} ions in different crystallographic sites and the occupational disorder, independently of the nature of the rare-earth ion [16][21]. In short, in this section we have analyzed in more detail the influence of the rare-earth magnetic interaction and have explained qualitatively the behavior features observed for different *R* substitutions.

5. Conclusions

Polycrystalline $RFeTi_2O_7$ (R = Eu, Gd, Dy, Ho, and Er) were produced by ceramic sintering at 1250 K and have been investigated using X-ray powder diffraction, and further characterized by specific heat, magnetization and frequency dependent ac susceptibility measurements.

The X-ray measurement indicates that $RFeTi_2O_7$ is orthorhombic, space group *Pcnb* at 300 K. The specific features of the structural characterization include the availability of the different non-equivalent positions for the magnetic Fe^{3+} ions in the unit cell of this material. The random site occupancy of the mixed octahedral sites (Ti/Fe) in all compounds, indicating a disorder of the magnetic iron ions distribution was observed.

The disorder and the competing magnetic interactions in $RFeTi_2O_7$ system leads to the formation of spin glass magnetic state at low temperatures. The $RFeTi_2O_7$ compound with the predominantly antiferromagnetic coupling undergoes a spin glass transition at the temperature T_{SG} depending strongly on the value of a static magnetic field.

The results of the temperature dependence of the heat capacity measurements show that no anomalies are observed in the temperature range of 2.0 – 100 K. So there are no long range ordering transitions in $RFeTi_2O_7$ compound. The transition to as spin-glass state is manifested with a very broad contribution centered at 5 – 10 K.

The thorough comparison of the spin glass properties of both, the series for R = Eu, Gd, Dy, Ho and Er, together with previous results for Tb and Lu, Tm and Yb, has drawn a picture of the active role played by rare earth in insulated spin glasses containing a 3d metal, Fe^{3+} and a 4f rare earth ion, R^{3+}. Magnetic rare earth ions participate in the spin glass transition through the interaction with the Fe^{3+} lattice. The stronger the anisotropy, the larger effect, evenly increasing the spin glass transition temperature and the coercive field below the transition. Anisotropy of the rare earth ion also influences the dynamics of the spin glass transition, slowing down the characteristic spin relaxation time to values typical of cluster glass. The substitution of non-magnetic Lu by high anisotropic rare earth ions, favours the formation of clusters with slower spin relaxation times.

The observed dependence in the spin glass transition as a function of the different rare earth substitution has been rationalized in the frame of molecular field theory of two sublattices. The estimation of R-Fe interaction from high temperature data extrapolation is in agreement with observed variations, validating the approach, despite its limitations.

As a final conclusion, magnetic rare earth ions participate in the spin glass state of $RFeTi_2O_7$ compounds modulating its properties. High anisotropic rare earth ions show a

larger increase of the spin glass transition temperature mediated by the anisotropic superexchange interaction with Fe^{3+} ions, with a slowed down dynamics.

Therefore, this work provides original relevant information of the interplay of interactions in insulating spin glasses containing both, rare-earth and transition metal ions.

Acknowledgements

This study has been financed by MECOM Projects MAT2014-53921-R, MAT2017-83468-R and DGA IMANA E34. Authors would like to acknowledge the use of Servicio General de Apoyo a la Investigación-SAI, Universidad de Zaragoza.

References

[1] I.Y. Korenblit, E.F. Shender, Sov. Phys. Uspekhi 32 (1989) 139–162.

[2] J.A. Mydosh, Spin-Glasses: An Experimental Introduction, Taylor&Francis, 1993.

[3] J.A. Mydosh, Reports Prog. Phys. 78 (2015) 52501.

[4] G.A. Petrakovskii, K.S. Aleksandrov, L.N. Bezmaternikh, S.S. Aplesnin, B. Roessli, F. Semadeni, A. Amato, C. Baines, J. Bartolomé, M. Evangelisti, Phys. Rev. B 63 (2001) 184425.

[5] H. Kawamura, T. Taniguchi, Handb. Magn. Mater. 24 (2015) 1–137.

[6] H. Akamatsu, J. Kawabata, K. Fujita, S. Murai, K. Tanaka, Phys. Rev. B 84 (2011) 144408/1-8.

[7] H. Akamatsu, K. Fujita, S. Murai, K. Tanaka, Phys. Rev. B 81 (2010) 014423/1-9.

[8] V. V Eremenko, V.A. Sirenko, A. Baran, E. Čižmár, A. Feher, J. Phys. Condens. Matter 30 (2018) 205801.

[9] R. Mathieu, A. Asamitsu, Y. Kaneko, J.P. He, Y. Tokura, Phys. Rev. B 72 (2005) 014436.

[10] M.B. Salamon, M. Jaime, Rev. Mod. Phys. 73 (2001) 583–628.

[11] M.-H. Phan, T.-L. Phan, T.-N. Huynh, S.-C. Yu, J.R. Rhee, N. Van Khiem, N.X. Phuc, J. Appl. Phys. 95 (2004) 7531–7533.

[12] N. Hasselmann, A.H. Castro Neto, C. Morais Smith, Phys. Rev. B 69 (2004) 014424.

[13] A. Malinowski, V.L. Bezusyy, R. Minikayev, P. Dziawa, Y. Syryanyy, M. Sawicki, Phys. Rev. B 84 (2011) 024409/1-17.

[14] A. Arauzo, N. V. Kazak, N.B. Ivanova, M.S. Platunov, Y. V. Knyazev, O.A. Bayukov, L.N. Bezmaternykh, I.S. Lyubutin, K. V. Frolov, S.G. Ovchinnikov, J. Bartolomé, J. Magn. Magn. Mater. 392 (2015) 114–125.

[15] H. Maletta, G. Aeppli, S.M. Shapiro, J. Magn. Magn. Mater. 31–34 (1983) 1367–1372.

[16] T. V. Drokina, G.A. Petrakovskii, M.S. Molokeev, A. Arauzo, J. Bartolomé, in:, Phys. Procedia, 2015, pp. 580–588.

[17] T. V. Drokina, G.A. Petrakovskii, D.A. Velikanov, M.S. Molokeev, Solid State Phenom. 215 (2014) 470–473.

[18] T. V Drokina, G.A. Petrakovskii, M.S. Molokeev, D.A. Velikanov, O.N. Pletnev, O.A. Bayukov, Phys. Solid State 55 (2013) 2037–2042.

[19] G.A. Petrakovskii, T. V. Drokina, A.L. Shadrina, D.A. Velikanov, O.A. Bayukov, M.S. Molokeev, A. V. Kartashev, G.N. Stepanov, Phys. Solid State 53 (2011) 1855–1858.

[20] T. V. Drokina, G.A. Petrakovskii, M.S. Molokeev, D.A. Velikanov, Phys. Solid State 60 (2018) 532–536.

[21] T. V. Drokina, G.A. Petrakovskii, O.A. Bayukov, M.S. Molokeev, J. Bartolomé, A. Arauzo, J. Magn. Magn. Mater. 440 (2017) 41–43.

[22] G.A. Petrakovskii, T. V. Drokina, D.A. Velikanov, O.A. Bayukov, M.S. Molokeev, A. V. Kartashev, A.L. Shadrina, A.A. Mitsuk, Phys. Solid State 54 (2012) 1813–1816.

[23] R. Mathieu, Y. Tokura, J. Phys. Soc. Japan 76 (2007) 124706.

[24] Y. Okimoto, H. Matsuzaki, Y. Tomioka, I. Kezsmarki, T. Ogasawara, M. Matsubara, H. Okamoto, Y. Tokura, J. Phys. Soc. Japan 76 (2007) 043702.

[25] C.S. Hong, W.S. Kim, E.O. Chi, N.H. Hur, Y.N. Choi, Chem. Mater. 14 (2002) 1832–1838.

[26] M. Andruh, P. Porchers, Inorg. Chem. 32 (1993) 1616–1622.

[27] A. Salamat, P.F. McMillan, S. Firth, K. Woodhead, A.L. Hector, G. Garbarino, M.C. Stennett, N.C. Hyatt, Inorg. Chem. 52 (2013) 1550–1558.

[28] J.G. Rau, M.J.P.P. Gingras, Phys. Rev. B 98 (2018) 054408/1-24.

[29] M. Ruminy, E. Pomjakushina, K. Iida, K. Kamazawa, D.T. Adroja, U. Stuhr, T. Fennell, Phys. Rev. B 94 (2016) 024430.

[30] T. Haku, M. Soda, M. Sera, K. Kimura, S. Itoh, T. Yokoo, T. Masuda, J. Phys. Soc. Japan 85 (2016) 034721.

[31] A. Bertin, Y. Chapuis, P. Dalmas De Réotier, A. Yaouanc, J. Phys. Condens. Matter 24 (2012)

256003.

[32] H. Cao, A. Gukasov, I. Mirebeau, P. Bonville, C. Decorse, G. Dhalenne, Phys. Rev. Lett. 103 (2009) 056402/1-4.

[33] I. Mirebeau, P. Bonville, M. Hennion, Phys. Rev. B 76 (2007) 184436.

[34] P. Dasgupta, Y. Jana, D. Ghosh, Solid State Commun. 139 (2006) 424–429.

[35] J.E. Greedan, J. Alloys Compd. 408–412 (2006) 444–455.

[36] S. Rosenkranz, A.P. Ramirez, A. Hayashi, R.J. Cava, R. Siddharthan, B.S. Shastry, J. Appl. Phys. 87 (2000) 5914.

[37] J.R.L. de Almeida, D.J. Thouless, J. Phys. A. Math. Gen. 11 (1978) 983–990.

[38] M. Gabay, G. Toulouse, Phys. Rev. Lett. 47 (1981) 201–204.

[39] D.N.H. Nam, R. Mathieu, P. Nordblad, N. V. Khiem, N.X. Phuc, Phys. Rev. B 62 (2000) 8989–8995.

[40] K. Vijayanandhini, C. Simon, V. Pralong, V. Caignaert, B. Raveau, Phys. Rev. B 79 (2009) 22440/1-10.

[41] S. Pakhira, C. Mazumdar, R. Ranganathan, S. Giri, M. Avdeev, Phys. Rev. B 94 (2016) 104414/1-15.

[42] P. Bag, P.R. Baral, R. Nath, Phys. Rev. B 98 (2018) 144436.

[43] E. Belorizky, M.A. Fremy, J.P. Gavigan, D. Givord, H.S. Li, J. Appl. Phys. 61 (1987) 3971–3973.

[44] K.P. Belov, A.K. Zvezdin, A.M. Kadomtseva, in:, I.M. Khalatnikov (Ed.), Phys. Rev., 1987, pp. 117–222.